Deformation response of conformally coated carbon nanotube forests

Parisa Pour Shahid Saeed Abadi[1], Matthew R Maschmann[2,3],
Jeffery W Baur[2], Samuel Graham[1,4] and Baratunde A Cola[1,4]

[1] George W. Woodruff School of Mechanical Engineering, Georgia Institute of Technology,
771 Ferst Drive, Atlanta, GA 30332, USA
[2] Air Force Research Laboratory, Materials and Manufacturing Directorate, AFRL/RX,
Wright-Patterson Air Force Base, OH 45433, USA
[3] Universal Technology Corporation, Beavercreek, OH 45432, USA
[4] School of Materials Science and Engineering, Georgia Institute of Technology,
771 Ferst Drive, Atlanta, GA 30332, USA

E-mail: cola@gatech.edu and sgraham@gatech.edu

Abstract

The deformation mechanism and mechanical properties of carbon nanotube (CNT) forests conformally coated with alumina using atomic layer deposition (ALD) are investigated using *in situ* and *ex situ* micro-indentation. While micro-indentation of a CNT forest coated with a thin discontinuous layer using 20 ALD cycles results in a deformation response similar to the response of uncoated CNT forests, a similar test on a CNT forest coated with a sufficiently thick and continuous layer using 100 ALD cycles causes fracture of both the alumina coatings and the core CNTs. With a 10 nm coating, 4-fold and 14-fold stiffness increases are measured using a flat punch and a Berkovich tip, respectively. Indentation testing with the Berkovich tip also reveals increased recoverability at relatively low strains. The results show that ALD coated CNT forests could be useful for applications that require higher stiffness or recoverability. Also, fracturing of the nanotubes shows that upper limits exist in the loading of conformally coated CNT forests.

S Online supplementary data available from stacks.iop.org/Nano/24/475707/mmedia

(Some figures may appear in colour only in the online journal)

1. Introduction

Coated CNTs have many potential applications such as optical, electronic, catalytic, sensing, and magnetic materials as well as reinforcement in composite materials, and have hence attracted the attention of many researchers [1–19]. Different coating methods such as physical vapor deposition [10, 11], chemical vapor deposition [5, 7], electroless plating [1, 3], and atomic layer deposition [4, 15–19] have been employed to coat CNTs. Moreover, coating CNT forests could be a means for tailoring their mechanical behavior by reinforcing individual CNTs and strengthening the contact forces between them. Coating CNTs after growth may be a more controllable means to alter forest behavior than by altering a CNT growth recipe that may simultaneously alter characteristics such as density, tortuosity, and entanglement [20, 21].

Mechanical properties and the deformation mechanisms of CNT forests have been extensively investigated [20–38]. *In situ* indentation experiments have revealed that buckling and shear offset formation are the most prominent deformations in the indentation of CNT forests. Despite significant recent attention to the visualization and characterization of the mechanical behavior of pristine CNT forests, the deformation and failure mechanism of coated CNT forests are not well known. Abadi *et al* [39] found that coating the top surface of CNT forests with a thin layer of aluminum causes delamination of the CNTs from the growth substrate under flat punch indentation. Raney *et al* [21] coated CNT forests with SnO_2 and MnO_2 nanoparticles and tested the coated CNT forests in compression. They reported increased energy dissipation in the CNT forests owing to the nanoparticle coating. The mechanical behavior of conformally coated

CNT forests (i.e., CNTs coated from top to bottom with a continuous layer of a second material) could be different from the behavior of CNT forests coated with a film on the top surface or with discrete particles along their height. This requires an in-depth investigation with the visualization of deformation and is the focus of this study.

Here, the mechanical behavior of CNT forests coated with different thicknesses of aluminum oxide (alumina) is reported. Coating is performed using atomic layer deposition (ALD), which is a chemical vapor phase deposition technique capable of depositing high-purity conformal coatings on high aspect ratio structures. It relies on the subsequent self-limiting deposition of alternate atomic layers. Alumina was selected as a common ALD material which has been shown to behave well as a seed layer for functionalizing the CNTs [5], isolating and insulating CNTs [5], and enhancing the stability and capacity of CNTs as an anode in Li-ion batteries [7]. *In situ* flat punch indentation of the hybrid structures was performed to observe the mechanical behavior. Furthermore, *ex situ* flat punch and Berkovich indentation testing was performed to quantify the stiffness and recoverability of the hybrid structures. We report multiple local buckling events at the bottom of CNT forests with a thin, discontinuous alumina coating produced by 20 ALD cycles, which is similar to the deformation of uncoated CNT forests. CNT forests coated by 100 ALD cycles (10–15 nm coating), however, failed by fracture of alumina/CNT nanotubes. Increases in the stiffness of CNT forests were measured using *ex situ* flat punch and Berkovich indentation of CNT forests. The amount of increase in stiffness is in the range predicted by the theories of bending and axial compression of individual CNTs. In addition, Berkovich indentation of the CNT forest coated with 10 nm alumina showed an increased recoverability compared to the CNT forest without coating. The observed fracture should be taken into account for determination of the load limit on coated CNT forests. The new results could also be a baseline for designing new structures for applications that require higher stiffness or recoverability.

2. Experimental details

2.1. CNT forest growth

An Aixtron Black Magic chemical vapor deposition (CVD) system was used to grow CNTs on Si substrates coated with Ti (30 nm)/Al (10 nm)/Fe (3 nm) as a catalyst stack. A low-pressure CVD (LPCVD) recipe was used with a growth temperature of ~750 °C and acetylene as the carbon source gas. The chamber pressure was approximately 10 mbar using a mixture of C_2H_2 and H_2 with flow rates of 100 and 700 sccm respectively. Growth times of 2 and 3.5 min were used and produced 10 and 30 μm tall CNT forests. The CNTs were multiwall CNTs with diameter ranges determined by transmission electron microscope (TEM) to be 7.2 ± 1.4 nm. The average number of walls was measured to be six. TEM images are provided in previous work [20].

2.2. Atomic layer deposition

ALD was carried out in a Cambridge NanoTech ALD system at 250 °C. Trimethylaluminum (TMA) and water were used as the sources of aluminum and oxygen, respectively. Every alumina deposition cycle included TMA dosing, Ar purging, water dosing, and Ar purging. The exposure and purging times in each cycle were 30 and 45 s respectively. Alumina coatings with different thicknesses were deposited using 20, 50, and 100 cycles, respectively. The deposition rate was measured to be approximately 1–1.6 Å per cycle.

2.3. Mechanical testing

In situ flat punch indentation was performed to visualize the deformation mechanism under compression loading. A micro-indenter with a tip cross section of 40 μm × 40 μm was used to indent the edge of the CNT forests in a scanning electron microscope (SEM). To visualize the deformation, a piece-wise displacement scheme was used in which after each 750 nm of displacement the indenter tip was held at a constant displacement while the SEM rastered a micrograph with a resolution of 3000 × 3000 pixels. Each micrograph acquisition was 60–90 s in duration. The indenter tip traveled at a displacement rate of 250 nm s^{-1} between displacement steps.

Ex situ indentation testing was done using two indenter types; a Berkovich tip and a flat punch with a 30 μm diameter circular cross section. A minimum of six measurements to a depth of 2–3 μm with a loading rate of 850 μN s^{-1} were performed using both tips to measure the stiffness. Then, scanning probe microscopy (SPM) was performed on the locations indented by the Berkovich tip to measure the size and depth of the permanent imprints for calculation of recoverability. SPM was performed by moving the Berkovich tip across the indented area while controlling the height to maintain a constant force of 2 nN.

3. Results and discussion

3.1. Morphological characterization

Characterization of the morphology of the coated CNTs was performed using SEM. All CNT forests were coated from root to top. The coating is discontinuous in the case of 20 ALD cycles (figure 1(a)). The nonuniformity is because without functionalization of CNTs there is a lack of nucleation sites. The uneven deposition due to the lack of functionalization has also been observed elsewhere [40]. Note that the CNT forests were coated without functionalization in order to prevent any effects of functionalization procedures (e.g., plasma or acid treatments) on the morphology and mechanical behavior of CNT forests. In the case of CNT forests coated using 100 ALD cycles, the majority of CNTs were continuously coated with an alumina layer with an approximate thickness of 10–16 nm. Figure 1(b), for instance, shows a CNT forest coated by 100 ALD cycles with a diameter range of 39 ± 7 (i.e., an average coating thickness of 16 nm). The
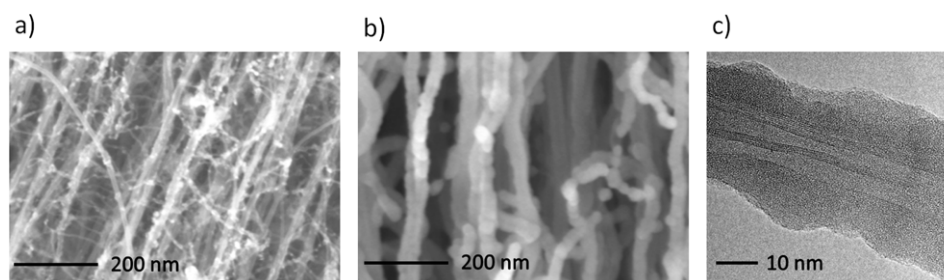
Figure 1. Morphology of alumina-coated carbon nanotubes. (a) SEM image of a CNT forest coated by 20 ALD cycles; uneven coating, (b) SEM image of a CNT forest coated by 100 ALD cycles; continuous coating, and (c) TEM image of a CNT forest coated by 100 ALD cycles.

thickness of the coating layer was estimated by subtracting the average radius of uncoated CNT—7.2 ± 1.4 nm as measured in TEM—from the average radius of coated CNTs. Therefore, the deposition rate is calculated to be in the range of 1–1.6 Å per cycle. Diameter measurements in SEM micrographs showed that the difference between the average diameter of nanotubes at the top and bottom of the CNT forests does not exceed 3%. This shows that in CNT forests up to the height of 30 μm, the penetration of the precursors into the CNT forests is sufficient to create nanotubes without a significant change of diameter from top to bottom. TEM images taken from the CNTs coated using 100 ALD cycles showed continuous coatings with some nonuniformity in the thickness (figure 1(c)). Other characterization results such as density measurement and x-ray photoelectron spectroscopy are provided in the supplementary data (available at stacks. iop.org/Nano/24/475707/mmedia).

3.2. In situ mechanical characterization

3.2.1. Deformation mechanism of 10 μm tall CNT forests with different coating thicknesses. First, indentation testing was performed on three CNT forests, all with the same height (10 μm) but coated by different numbers of ALD cycles (no coating, 20 cycles and 100 cycles). The deformations to similar strains of 30–50% are shown in figure 2. Both the uncoated CNT forest (figure 2(a)) and the one coated by 20 cycles (figure 2(b)) exhibited formation of local periodic buckles starting from the bottom of the CNT forest. The deformation was similar to the deformation of uncoated CNT forests grown with the same recipe in a prior study [20]. Multiple buckles close to the substrate in figure 2(b) are magnified in figure 2(c), with the topmost buckle being the most visible. Highly deformed coated CNTs in figure 2(c) are magnified in figure 2(d). The high-magnification SEM images show no discernible fracture of nanotubes in this CNT forest, even in the highly deformed regions. Figure 2(e) shows the deformation of the CNT forest coated by 100 ALD cycles. Although the indentation depth was similar to the other two cases (no coating and coated by 20 cycles), different deformation and failure mechanisms were observed; the nanotubes fractured in a brittle manner. The nanotubes that moved toward the viewing pane are magnified in figures 2(f) and (g). Bare CNTs are observable in the high-magnification images. Arrows are used to indicate a few of the bare CNTs

in both figures 2(f) and (g). The fractured ends of the CNTs which are easily discernible in figure 2(g) show that not only the alumina coating but also the CNTs are fractured. While the buckles in the other two CNT forests (no coating and coated by 20 ALD cycles) extended horizontally beyond the width of the indenter due to the interaction between CNTs, the deformation and fracture in the CNT forest coated by 100 ALD cycles are confined to the area directly under the indenter. This is likely because the fracture of the connections between CNTs under the edge of the indenter requires smaller loads than bending of the surrounding CNTs.

3.2.2. Deformation mechanism of 30 μm tall CNT forests with different coating thicknesses. To examine the deformation and failure mechanism in taller CNT forests, micro-indentation experiments were performed on 30 μm tall CNT forests similar to those performed on 10 μm tall CNT forests. The deformation mechanism for an uncoated CNT forest, and those coated by 20 and 100 cycles are shown in figures 3(a)–(c) respectively. Similar to the case of 10 μm tall CNT forests, 30 μm tall CNT forests without coating and coated by 20 ALD cycles were deformed by the formation of multiple local buckles close to the substrate (figures 3(a) and (b)) while the CNT forest coated by 100 ALD cycles failed by fracture of the nanotubes (figure 3(c))—both alumina coating and CNTs. Also similar to the case of 10 μm tall CNT forests, the deformations in the case of no coating and thin coating were extended beyond the area directly under indenter, while the deformations in the case of thick coating were confined to the area directly under the indenter.

SEM images of the step-by-step deformation and fracture of the 30-μm tall CNT forests coated by 100 ALD cycles are featured in figures 4(a)–(e) and the corresponding points on the load–displacement curve are marked in figure 4(f). The jagged parts of the load–displacement curve are related to relaxation at the time intervals when the tip displacement was fixed in order to collect SEM images. Point (a) shows the start of indentation of the CNT forest. The first visible deformation occurred at point (b), where a wrinkle was formed. The wrinkle progress led to fracture of the nanotubes, and can be distinguished more clearly in points (c)–(e). The top fractured section moved further away from the viewing pane and the fractured tips of the bottom section moved toward the viewing pane. Formation of the wrinkle was associated with a small drop in load and a sudden displacement at
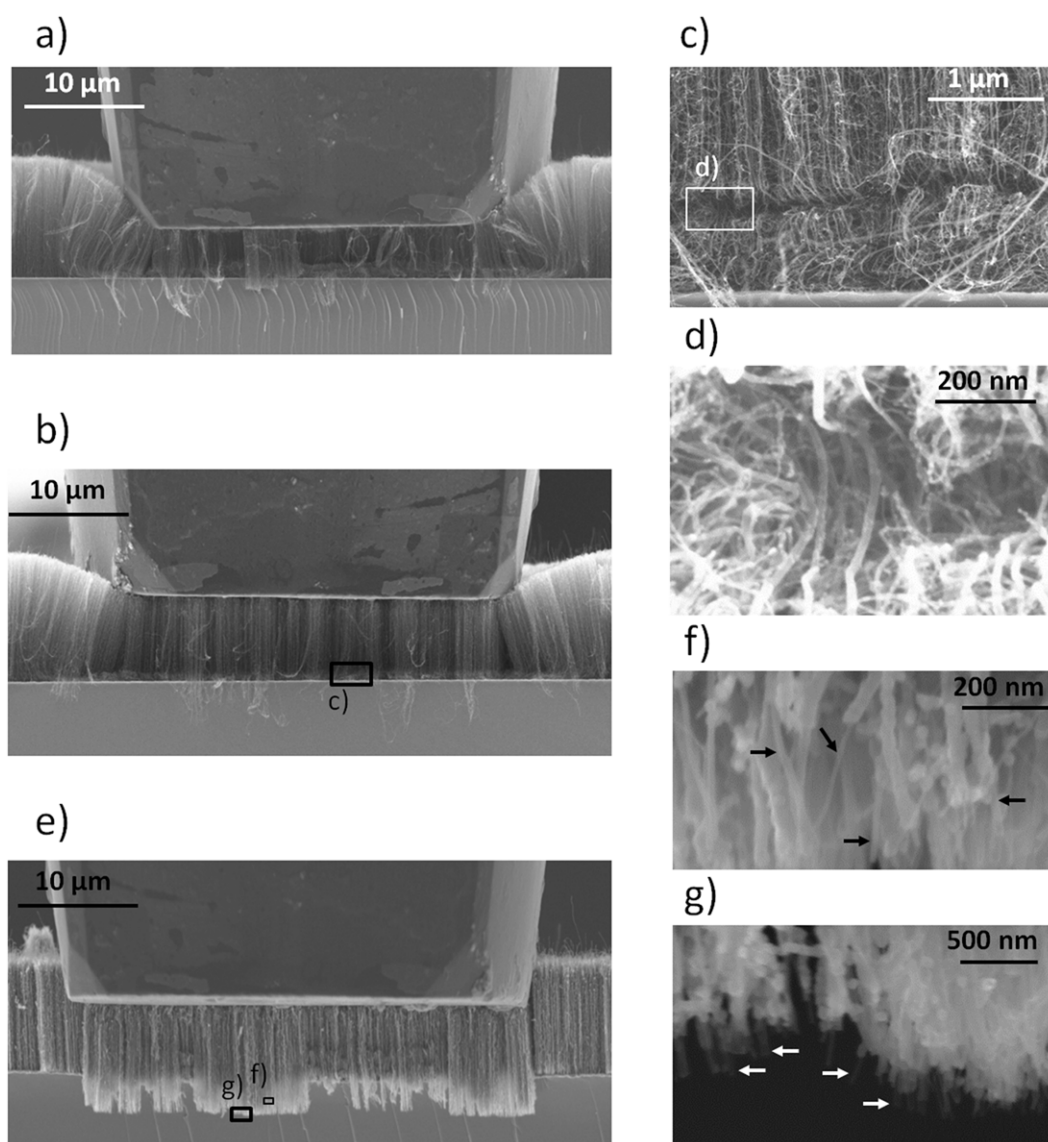
Figure 2. Deformed uncoated and alumina-coated 10 μm tall CNT forests after micro-indentation. (a) Uncoated CNT forest buckled from bottom, (b) CNT forest coated by 20 ALD cycles buckled from bottom, similar to an uncoated CNT forest, (c) magnified view of the area inside the rectangle in (b), showing the multiple buckles close to substrate, (d) magnified view of the area inside the rectangle in (c), showing curved CNTs in the topmost buckle with no fracture, (e) CNT forest coated by 100 ALD cycles, showing nanotube fracture, (f), and (g) magnified view of the rectangles in (e), showing fractured nanotubes—arrows indicate some of the bare CNTs pulled out of the alumina coating.

point (b), while the complete fracture of the CNT/alumina nanotubes was associated with a larger drop in load and sudden displacement at point (c). Point (d) shows the indenter at maximum displacement before the start of unloading. Point (e) shows the unloaded sample with almost no recovery, as expected due to fracture. Videos of the indentation on the uncoated CNT forest and the one with 100 ALD cycles are provided in the supplementary data (available at stacks.iop. org/Nano/24/475707/mmedia).

3.2.3. Fracture mechanism. In the case of 20 ALD cycles, alumina deposits on the CNTs in the form of nanoparticles, as shown in figure 2(d). This causes the deformation mechanism of the CNT forest coated by 20 ALD cycles to remain similar to the deformation mechanism in an uncoated CNT

forest. In the case of 100 ALD cycles, however, the coating is continuous and an alumina nanotube forms around each CNT (figures 2(f) and (g)). Alumina is a material with low toughness [41] and alumina nanotubes do not have the flexibility similar to CNTs to fold and buckle without fracturing; hence the observed fracture of CNTs coated with a continuous film of alumina was not unexpected. The consequent fracturing of CNTs, however, requires further clarification. Fracture due to tension loading as illustrated in figure 5 is a likely scenario for CNT fracture. The CNT bridges the fractured alumina nanotube pieces after fracturing of the alumina coating (figure 5(b)) but eventually fractures after stress in the CNT exceeds its tensile strength (figure 5(c)). Bare CNTs shown in figure 5(d) are the experimental evidence of this elongation and bridging. The
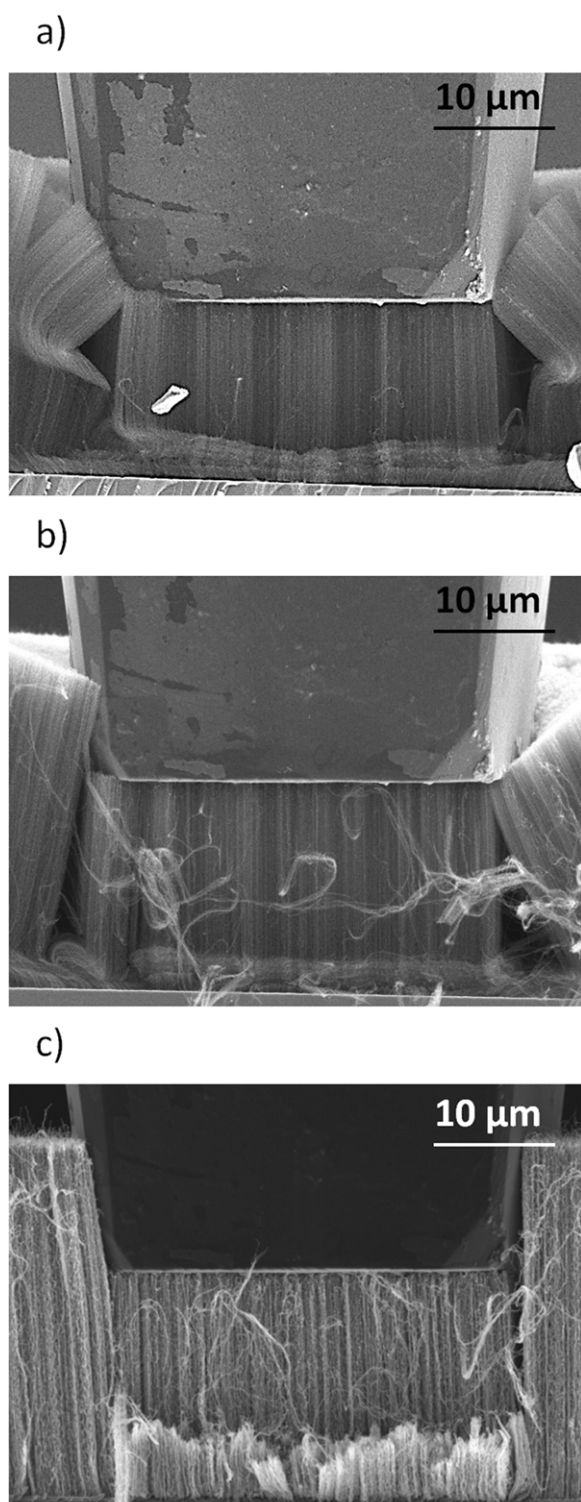
a)

b)

c)

Figure 3. Deformed uncoated and alumina-coated 30 μm tall CNT forests after micro-indentation. (a) Uncoated CNT forest buckled from bottom, (b) CNT forest coated by 20 ALD cycles buckled from bottom, similar to uncoated CNT forest, (c) CNT forest coated by 100 ALD cycles, showing nanotube fracture.

bridging is believed to be similar to the CNT bridging in CNT–alumina composites. For instance, CNTs bridging a crack in a CNT-amorphous alumina powder have been demonstrated [42]. This mechanism has been proposed to increase the toughness of the ceramic composites. The

fracture in the CNTs probably initiates from the defects usually existing in CVD-grown CNTs [33, 43] or from defects caused by contact with the fractured edge of the alumina nanotube. The highly defective structure of CVD-grown CNTs results in a wide range of tensile strength. The tensile strength has been reported to be in the range of approximately 20–200 GPa for individual CVD-grown CNTs with a diameter range of 20–25 nm [33, 44], with half of the data being between approximately 50–150 GPa. It is not possible to get a reasonable estimation of the tensile stresses at the fracture locations due to the complexities of the structure. However, tensile stresses close to the range measured for MWCNTs [33, 44] (20–200 GPa) are expected in the bare CNTs that fractured.

3.3. Ex situ mechanical characterization; stiffness and recoverability measurement

Two indenter types, a Berkovich tip and a flat punch with a 30 μm diameter circular cross section, were used for *ex situ* mechanical characterization. The unloading stiffness (the slope of the initial part of unloading curve) was measured for indentation by both tips. The results are shown in figure 6, with a schematic demonstration of tip geometries and CNT deformations using each tip. A flat punch compresses the CNTs downward while an angled tip such as a Berkovich tip deforms CNTs by a combination of downward compression and bending to the sides. This fact was the motivation for using two indenters—i.e., to investigate the effect of CNT coating on the stiffness in two modes of deformation caused by the two indenters. A significant increase in the stiffness due to coating was measured. The Berkovich tip measured lower stiffness values compared to the flat punch. This is expected because of the smaller contact area between the CNTs and the Berkovich tip. The increase in stiffness with 10 nm coating was measured by the Berkovich tip to be 14-fold and by the flat punch to be 4-fold. The effects of coating on the stiffness of CNTs were compared with theoretical estimations using simple compression and bending theories to facilitate understanding of the measured differences. In a pure axial compression mode, stiffness is proportional to the product of Young's modulus and area, *EA*, while in a pure bending mode it is proportional to the product of Young's modulus and bending moment of inertia, *EI*. Young's modulus has been measured to be in the range 0.8–1.3 TPa for multiwall CNTs [45–47] and 170–180 GPa for ALD alumina [48]. Calculations in this work were performed using 2.9 and 7.2 nm as the inner and outer diameters of CNTs (the average value measured in TEM images), 1 TPa as the Young's modulus of CNTs, and 180 GPa as the Young's modulus of ALD alumina. The results are listed in table 1 for a bare CNT and for a CNT coated with 5 and 10 nm alumina. Pure compression theory predicts a 4-fold increase in stiffness with a 10 nm alumina coating, while pure bending theory predicts a 40-fold increase. Both sets of experimental data (using flat punch and Berkovich tip) fall in the range predicted by the assumptions of pure compression and pure bending. The fact that the increase in stiffness measured by
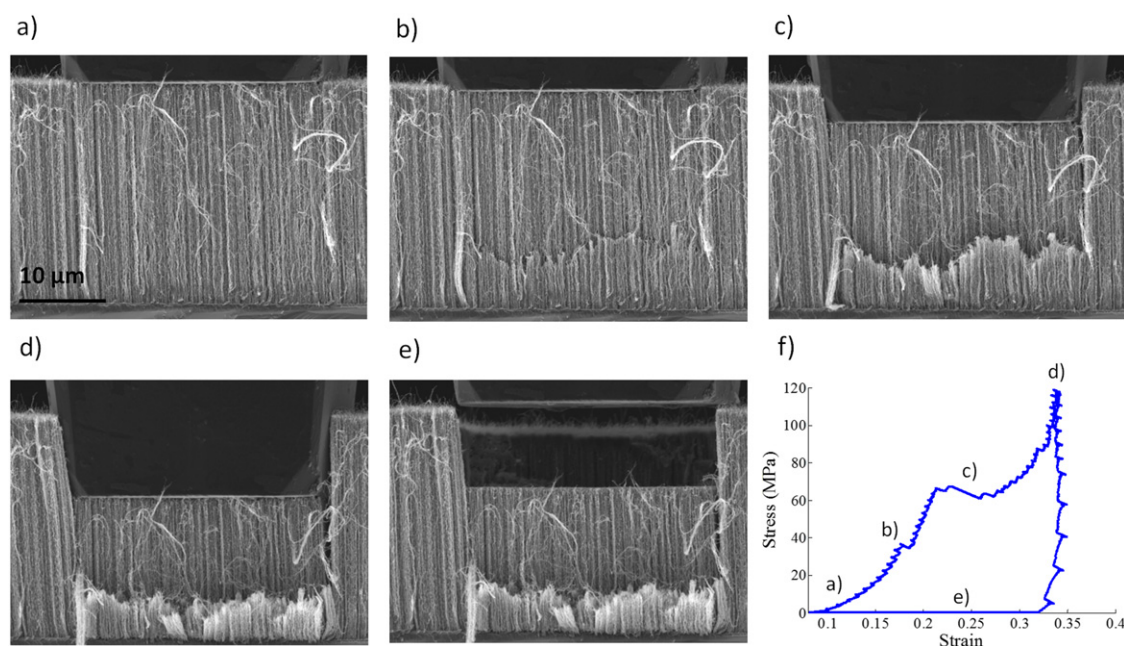
Figure 4. Deformation of a CNT forest coated by 100 ALD cycles. (a) Initiation of compression loading with no visible deformation, (b) after formation of a local buckle, (c) progress of the buckle leading to fracture of nanotubes, (d) maximum displacement of the indenter—broken nanotube tips are observable on the bottom section, (e) unloaded state, and (f) stress–strain curve with marked points associated with images (a)–(e).
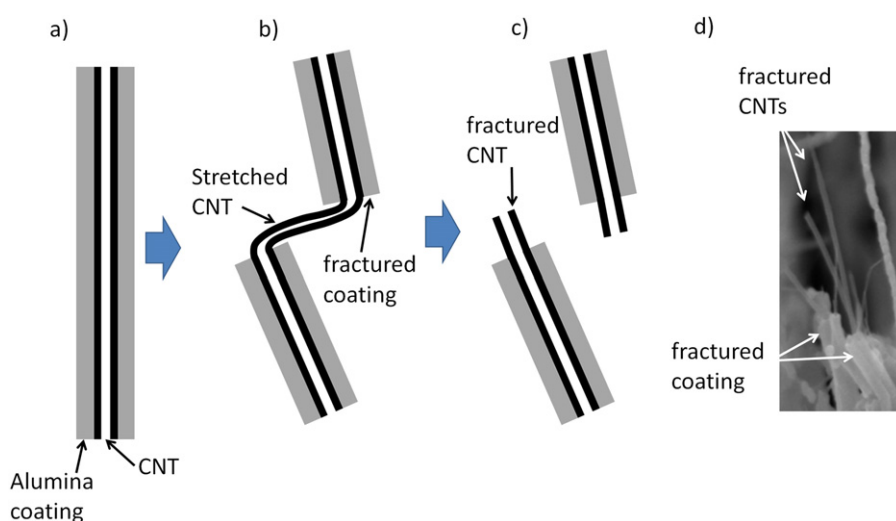

Figure 5. Fracture of a coated CNT. (a) A coated CNT before fracture, (b) after fracture of the coating, (c) after fracture of both coating and CNT, and (d) fractured alumina/CNT after indentation of a 30 μm tall CNT forest coated using 100 ALD cycles.

the Berkovich tip falls between the values predicted by the pure compression and pure bending theories is due to the fact that the response is a combination of both deformation modes. The value measured by flat punch is the same as the prediction by pure compression theory. This is likely because the release of the axial loads is dominant in the initial portion of the unloading. The increase in the collective stiffness could be due to the increase in the stiffness of individual CNTs or due to the increase in interlocking of CNTs by coating. However, the results obtained by the flat punch indentation probably mean that the former is more significant when the coating is as thick as 10 nm.

Table 1. Theoretical estimation of *EA* and *EI* for bare and coated CNTs.

	EA (μN)	*EI* ($\times 10^{-17}$ μN m^2)
CNT	34	13
CNT coated with 5 nm alumina	67	88
CNT coated with 10 nm alumina	130	490

The locations indented by the Berkovich tip were imaged using SPM to measure the size and depth of the permanent imprints. SPM was performed by moving the Berkovich tip across the indented area while controlling the height to
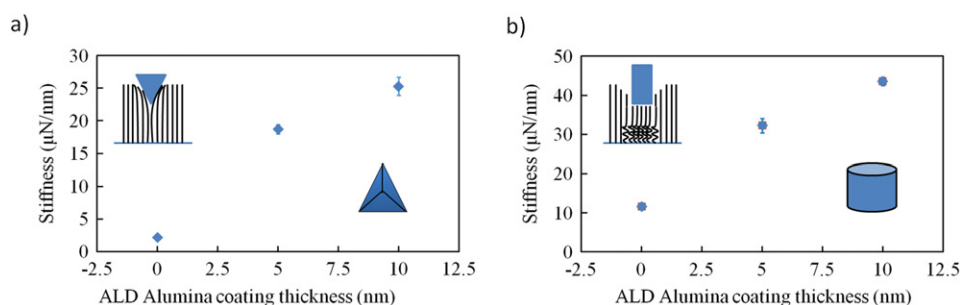
6

Figure 6. Stiffness data for CNT forests with no coating and 5 and 10 nm coating measured by (a) a Berkovich tip, and (b) a flat punch. Schematic of the tip shapes and deformation mechanism using the two indenters are shown in the figures.
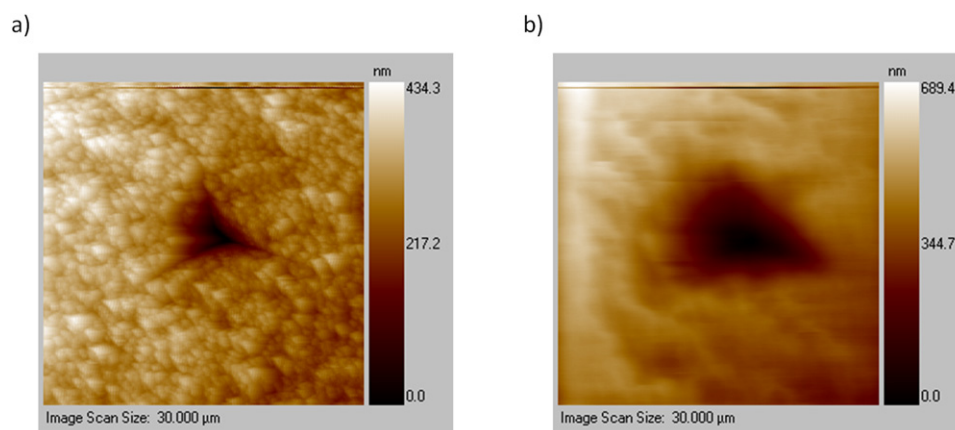

Figure 7. Permanent deformations after indentation by a Berkovich tip and scanned using the same tip. (a) The CNT forest with 10 nm coating, and (b) the uncoated CNT forest.

maintain a constant force of 2 nN. The size and depth of the imprints were smaller in the coated samples than the uncoated samples. This is shown for a CNT forest with 10 nm coating in figure 7. The maximum depth as shown in the scale bars was decreased by approximately 40% (from 689 to 434 nm) with the 10 nm coating. This is likely due to higher van der Waals (vdW) forces between bare CNTs compared to coated CNTs that keep them together when bent. The vdW forces are proportional to the Hamaker constant [49] which has been reported to be 15×10^{19} for alumina [50] compared to 47×10^{19} for graphite [51]. The greater restoring force resulting from the increased bending stiffness of the nanotubes could also have contributed to the increased recoverability. The recoverability was almost negligible in the case of flat punch indentation, due to the fracturing of nanotubes. In the case of Berkovich indentation, less fracturing is expected, since bending of CNTs is more prevalent.

of CNTs after fracture of the alumina nanotubes. The results of *ex situ* indentation testing indicated that a 10 nm coating increases the stiffness measured by a flat punch by 4-fold and the stiffness measured by a Berkovich tip by 14-fold. The difference is related to the fact that the stiffness measured by the flat punch originates predominantly from pure compression while the one measured by the Berkovich tip originates from a combination of bending and compression. Furthermore, recoverability of the deformation after Berkovich indentation, measured by scanning the indented area after testing, was 40% higher in a CNT forest with a 10 nm alumina coating compared to one without a coating. The information on both increased stiffness and recoverability could be useful for designing new hybrid structures. The load at which nanotubes fracture (e.g., 30–40 MPa for the case of 10–16 nm alumina coating) should be considered as the load limit of the structure.

4. Conclusions

Substantial changes in the deformation and properties of CNT forests were observed by ALD alumina coating as thin as 10–16 nm. *In situ* flat punch indentations showed that while a continuous layer of coating could cause fracture of a CNT/alumina hybrid nanostructure, thinner coatings that form particles on the CNTs do not change the deformation mechanism significantly. The fracture of CNTs coated with a continuous film of alumina is likely due to tensile loading

References

[1] Ang L, Hor T S A, Xu G, Tung C, Zhao S and Wang J 2000 *Carbon* **38** 363–72

[2] Hamdan A, Cho J, Johnson R, Jiao J, Bahr D, Richards R and Richards C 2010 *Nanotechnology* **21** 015702

[3] Kong F, Zhang X, Xiong W, Liu F, Huang W, Sun Y, Tu J and Chen X 2002 *Surf. Coat. Technol.* **155** 33–6

[4] Lee J, Min B, Cho K, Kim S, Park J, Lee Y, Kim N, Lee M, Park S and Moon J 2003 *J. Cryst. Growth* **254** 443–8

[5] Liu Z J, Xu Z, Yuan Z Y, Chen W, Zhou W and Peng L M 2003 *Mater. Lett.* **57** 1339–44

[6] McBride J, Yunus E and Spearing S 2010 *Eur. Phys. J. Appl. Phys.* **50** 507–13

[7] Morisada Y and Miyamoto Y 2004 *Mater. Sci. Eng.* A **381** 57–61

[8] Tripathi S M, Bholanath T S and Shantkriti S 2010 *Int. J. Control Autom.* **3** 53–64

[9] Wei X W, Song X J, Xu J, Ni Y H and Zhang P 2005 *Mater. Chem. Phys.* **92** 159–63

[10] Zhang Y, Franklin N W, Chen R J and Dai H 2000 *Chem. Phys. Lett.* **331** 35–41

[11] Zhang Y, Zhang Q, Li Y, Wang N and Zhu J 2000 *Solid State Commun.* **115** 51–5

[12] Chandrashekar A, Ramachandran S, Pollack G, Lee J S, Lee G S and Overzet L 2008 *Thin Solid Films* **517** 525–30

[13] Lahiri I, Oh S-M, Hwang J Y, Kang C, Choi M, Jeon H, Banerjee R, Sun Y-K and Choi W 2011 *J. Mater. Chem.* **21** 13621–6

[14] Gomathi A, Vivekchand S, Govindaraj A and Rao C 2005 *Adv. Mater.* **17** 2757–61

[15] Herrmann C, Fabreguette F, Finch D, Geiss R and George S 2005 *Appl. Phys. Lett.* **87** 123110

[16] Min Y S, Bae E J, Jeong K S, Cho Y J, Lee J H, Choi W B and Park G S 2003 *Adv. Mater.* **15** 1019–22

[17] Willinger M G, Neri G, Bonavita A, Micali G, Rauwel E, Herntrich T and Pinna N 2009 *Phys. Chem. Chem. Phys.* **11** 3615–22

[18] Farmer D B and Gordon R G 2006 *Nano Lett.* **6** 699–703

[19] Min Y-S, Bae E J, Park J B, Kim U J, Park W, Song J, Hwang C S and Park N 2007 *Appl. Phys. Lett.* **90** 263104

[20] Pour Shahid Saeed Abadi P, Hutchens S B, Greer J R, Cola B A and Graham S 2012 *Nanoscale* **4** 8

[21] Raney J R, Misra A and Daraio C 2011 *Carbon* **49** 3631–8

[22] McCarter C M, Richards R F, Mesarovic S D, Richards C D, Bahr D F, McClain D and Jiao J 2006 *J. Mater. Sci.* **41** 7872–8

[23] Qiu A, Bahr D F, Zbib A A, Bellou A, Mesarovic S D, McClain D, Hudson W, Jiao J, Kiener D and Cordill M J 2011 *Carbon* **49** 1430–8

[24] Malik H, Stephenson K J, Bahr D F and Field D P 2011 *J. Mater. Sci.* **46** 3119–26

[25] Mesarovic S D, McCarter C M, Bahr D F, Radhakrishnan H, Richards R F, Richards C D, McClain D and Jiao J 2007 *Scr. Mater.* **56** 157–60

[26] Qi H J, Teo K B K, Lau K K S, Boyce M C, Milne W I, Robertson J and Gleason K K 2003 *J. Mech. Phys. Solids* **51** 2213–37

[27] Cao A Y, Dickrell P L, Sawyer W G, Ghasemi-Nejhad M N and Ajayan P M 2005 *Science* **310** 1307–10

[28] Cao C, Reiner A, Chung C, Chang S H, Kao I, Kukta R V and Korach C S 2011 *Carbon* **49** 3190–9

[29] Hutchens S B, Hall L J and Greer J R 2010 *Adv. Funct. Mater.* **20** 2338–46

[30] Maschmann M R, Ehlert G J, Park S J, Mollenhauer D, Maruyama B, Hart A J and Baur J W 2012 *Adv. Funct. Mater.* **22** 4625

[31] Maschmann M R, Zhang Q, Wheeler R, Du F, Dai L and Baur J 2011 *ACS Appl. Mater. Interfaces* **3** 648–53

[32] Maschmann M R, Zhang Q H, Du F, Dai L M and Baur J 2011 *Carbon* **49** 386–97

[33] Barber A H, Andrews R, Schadler L S and Wagner H D 2005 *Appl. Phys. Lett.* **87** 203106

[34] Gao Y, Kodama T, Won Y, Dogbe S, Pan L and Goodson K E 2012 *Carbon* **50** 3789–98

[35] Nguyen J J, Bougher T L, Pour Shahid Saeed Abadi P, Sharma A, Graham S and Cola B A 2013 *J. Micro Nano-Manuf.* **1** 014501

[36] Lu Y, Joseph J, Maschmann M, Dai L and Baur J 2013 *Challenges in Mechanics of Time-Dependent Materials and Processes in Conventional and Multifunctional Materials* vol 2 (Berlin: Springer) pp 101–7

[37] Pathak S, Mohan N, Pour Shahid Saeed Abadi P, Graham S, Cola B and Greer J 2012 *J. Mater. Res.* **28** 984–97

[38] Pathak S, Lim E J, Pour Shahid Saeed Abadi P, Graham S, Cola B A and Greer J R 2012 *ACS Nano* **6** 2189–97

[39] Pour Shahid Saeed Abadi P, Hutchens S B, Greer J R, Cola B A and Graham S 2013 *Appl. Phys. Lett.* **102** 223103

[40] Guangyu Z, Xinran W, Xiaolin L, Yuerui L, Ali J and Dai H 2006 Carbon nanotubes: from growth, placement and assembly control to 60 mV/decade and sub-60 mV/decade tunnel transistors *Electron Devices Mtg., 2006, IEDM'06. Int. (11–13 Dec. 2006)* pp 1–4

[41] Gorczyca F E 1987 *Application of Metal Cutting Theory* (New York: Industrial Press) p 298

[42] Cha S I, Kim K T, Lee K H, Mo C B and Hong S H 2005 *Scr. Mater.* **53** 793–7

[43] Xie S, Li W, Pan Z, Chang B and Sun L 2000 *J. Phys. Chem. Solids* **61** 1153–8

[44] Andrews R, Jacques D, Rao A M, Derbyshire F, Qian D, Fan X, Dickey E C and Chen J 1999 *Chem. Phys. Lett.* **303** 467–74

[45] Wong E W, Sheehan P E and Lieber C M 1997 *Science* **277** 1971–5

[46] Demczyk B G, Wang Y M, Cumings J, Hetman M, Han W, Zettl A and Ritchie R O 2002 *Mater. Sci. Eng.* A **334** 173–8

[47] Salvetat J P, Bonard J M, Thomson N H, Kulik A J, Forro L, Benoit W and Zuppiroli L 1999 *Appl. Phys.* A **69** 255–60

[48] Tripp M K, Stampfer C, Miller D C, Helbling T, Hermann C F, Hierold C, Gall K, George S M and Bright V M 2006 *Sensors Actuators* A **130** 419–29

[49] Hiemenz P C and Rajagopalan R 1997 *Principles of Colloid and Surface Chemistry* 3rd edn (New York: Dekker) p 650

[50] Lefèvre G and Jolivet A 2009 Calculation of Hamaker constants applied to the deposition of metallic oxide particles at high temperature *Proc. Int. Conf. on Heat Exchanger Fouling and Cleaning, 2009* pp 120–4

[51] Lyklema J 2000 *Fundamentals of Interface and Colloid Science* vol 3 (San Diego: Academic)